

Indication of Electron Neutrino Appearance from an Accelerator-produced Off-axis Muon Neutrino Beam

K. Abe,⁴⁹ N. Abgrall,¹⁶ Y. Ajima,^{18,*} H. Aihara,⁴⁸ J.B. Albert,¹³ C. Andreopoulos,⁴⁷
 B. Andrieu,³⁷ S. Aoki,²⁷ O. Araoka,^{18,*} J. Argyriades,¹⁶ A. Ariga,³ T. Ariga,³
 S. Assylbekov,¹¹ D. Autiero,³² A. Badertscher,¹⁵ M. Barbi,⁴⁰ G.J. Barker,⁵⁶ G. Barr,³⁶
 M. Bass,¹¹ F. Bay,³ S. Bentham,²⁹ V. Berardi,²² B.E. Berger,¹¹ I. Bertram,²⁹ M. Besnier,¹⁴
 J. Beucher,⁸ D. Beznosko,³⁴ S. Bhadra,⁵⁹ F.d.M. Blaszczyk,⁸ A. Blondel,¹⁶ C. Bojchko,⁵³
 J. Bouchez,^{8,†} S.B. Boyd,⁵⁶ A. Bravar,¹⁶ C. Bronner,¹⁴ D.G. Brook-Roberge,⁵
 N. Buchanan,¹¹ H. Budd,⁴¹ D. Calvet,⁸ S.L. Cartwright,⁴⁴ A. Carver,⁵⁶ R. Castillo,¹⁹
 M.G. Catanesi,²² A. Cazes,³² A. Cervera,²⁰ C. Chavez,³⁰ S. Choi,⁴³ G. Christodoulou,³⁰
 J. Coleman,³⁰ W. Coleman,³¹ G. Collazuol,²⁴ K. Connolly,⁵⁷ A. Curioni,¹⁵ A. Dabrowska,¹⁷
 I. Danko,³⁸ R. Das,¹¹ G.S. Davies,²⁹ S. Davis,⁵⁷ M. Day,⁴¹ G. De Rosa,²³ J.P.A.M. de
 André,¹⁴ P. de Perio,⁵¹ A. Delbart,⁸ C. Densham,⁴⁷ F. Di Lodovico,³⁹ S. Di Luise,¹⁵
 P. Dinh Tran,¹⁴ J. Dobson,²¹ U. Dore,²⁵ O. Drapier,¹⁴ F. Dufour,¹⁶ J. Dumarchez,³⁷
 S. Dytman,³⁸ M. Dziewiecki,⁵⁵ M. Dziomba,⁵⁷ S. Emery,⁸ A. Ereditato,³ L. Escudero,²⁰
 L.S. Esposito,¹⁵ M. Fechner,^{13,8} A. Ferrero,¹⁶ A.J. Finch,²⁹ E. Frank,³ Y. Fujii,^{18,*}
 Y. Fukuda,³³ V. Galymov,⁵⁹ F. C. Gannaway,³⁹ A. Gaudin,⁵³ A. Gendotti,¹⁵ M.A. George,³⁹
 S. Giffin,⁴⁰ C. Giganti,¹⁹ K. Gilje,³⁴ T. Golan,⁵⁸ M. Goldhaber,^{6,†} J.J. Gomez-Cadenas,²⁰
 M. Gonin,¹⁴ A. Grant,⁴⁶ N. Grant,²⁹ P. Gumplinger,⁵² P. Guzowski,²¹ A. Haesler,¹⁶
 M.D. Haigh,³⁶ K. Hamano,⁵² C. Hansen,^{20,‡} D. Hansen,³⁸ T. Hara,²⁷ P.F. Harrison,⁵⁶
 B. Hartfiel,³¹ M. Hartz,^{59,51} T. Haruyama,^{18,*} T. Hasegawa,^{18,*} N.C. Hastings,⁴⁰
 S. Hastings,⁵ A. Hatzikoutelis,²⁹ K. Hayashi,^{18,*} Y. Hayato,⁴⁹ C. Hearty,^{5,§} R.L. Helmer,⁵²
 R. Henderson,⁵² N. Higashi,^{18,*} J. Hignight,³⁴ E. Hirose,^{18,*} J. Holeczek,⁴⁵ S. Horikawa,¹⁵
 A. Hyndman,³⁹ A.K. Ichikawa,²⁸ K. Ieki,²⁸ M. Ieva,¹⁹ M. Iida,^{18,*} M. Ikeda,²⁸ J. Ilic,⁴⁷
 J. Imber,³⁴ T. Ishida,^{18,*} C. Ishihara,⁵⁰ T. Ishii,^{18,*} S.J. Ives,²¹ M. Iwasaki,⁴⁸ K. Iyogi,⁴⁹
 A. Izmaylov,²⁶ B. Jamieson,⁵ R.A. Johnson,¹⁰ K.K. Joo,⁹ G.V. Jover-Manas,¹⁹ C.K. Jung,³⁴
 H. Kaji,⁵⁰ T. Kajita,⁵⁰ H. Kakuno,⁴⁸ J. Kameda,⁴⁹ K. Kaneyuki,^{50,†} D. Karlen,^{53,52}
 K. Kasami,^{18,*} I. Kato,⁵² E. Kearns,⁴ M. Khabibullin,²⁶ F. Khanam,¹¹ A. Khotjantsev,²⁶

D. Kielczewska,⁵⁴ T. Kikawa,²⁸ J. Kim,⁵ J.Y. Kim,⁹ S.B. Kim,⁴³ N. Kimura,^{18,*} B. Kirby,⁵
 J. Kisiel,⁴⁵ P. Kitching,¹ T. Kobayashi,^{18,*} G. Kogan,²¹ S. Koike,^{18,*} A. Konaka,⁵²
 L.L. Kormos,²⁹ A. Korzenev,¹⁶ K. Koseki,^{18,*} Y. Koshio,⁴⁹ Y. Kouzuma,⁴⁹ K. Kowalik,²
 V. Kravtsov,¹¹ I. Kreslo,³ W. Kropp,⁷ H. Kubo,²⁸ Y. Kudenko,²⁶ N. Kulkarni,³¹ R. Kurjata,⁵⁵
 T. Kutter,³¹ J. Lagoda,² K. Laihem,⁴² M. Laveder,²⁴ K.P. Lee,⁵⁰ P.T. Le,³⁴ J.M. Levy,³⁷
 C. Licciardi,⁴⁰ I.T. Lim,⁹ T. Lindner,⁵ R.P. Litchfield,^{56,28} M. Litos,⁴ A. Longhin,⁸
 G.D. Lopez,³⁴ P.F. Loverre,²⁵ L. Ludovici,²⁵ T. Lux,¹⁹ M. Macaire,⁸ K. Mahn,⁵²
 Y. Makida,^{18,*} M. Malek,²¹ S. Manly,⁴¹ A. Marchionni,¹⁵ A.D. Marino,¹⁰ J. Marteau,³²
 J.F. Martin,^{51,§} T. Maruyama,^{18,*} T. Maryon,²⁹ J. Marzec,⁵⁵ P. Masliah,²¹ E.L. Mathie,⁴⁰
 C. Matsumura,³⁵ K. Matsuoka,²⁸ V. Matveev,²⁶ K. Mavrokoridis,³⁰ E. Mazzucato,⁸
 N. McCauley,³⁰ K.S. McFarland,⁴¹ C. McGrew,³⁴ T. McLachlan,⁵⁰ M. Messina,³
 W. Metcalf,³¹ C. Metelko,⁴⁷ M. Mezzetto,²⁴ P. Mijakowski,² C.A. Miller,⁵² A. Minamino,²⁸
 O. Mineev,²⁶ S. Mine,⁷ A.D. Missert,¹⁰ G. Mituka,⁵⁰ M. Miura,⁴⁹ K. Mizouchi,⁵²
 L. Monfregola,²⁰ F. Moreau,¹⁴ B. Morgan,⁵⁶ S. Moriyama,⁴⁹ A. Muir,⁴⁶ A. Murakami,²⁸
 M. Murdoch,³⁰ S. Murphy,¹⁶ J. Myslik,⁵³ T. Nakadaira,^{18,*} M. Nakahata,⁴⁹ T. Nakai,³⁵
 K. Nakajima,³⁵ T. Nakamoto,^{18,*} K. Nakamura,^{18,*} S. Nakayama,⁴⁹ T. Nakaya,²⁸
 D. Naples,³⁸ M.L. Navin,⁴⁴ B. Nelson,³⁴ T.C. Nicholls,⁴⁷ K. Nishikawa,^{18,*} H. Nishino,⁵⁰
 J.A. Nowak,³¹ M. Noy,²¹ Y. Obayashi,⁴⁹ T. Ogitsu,^{18,*} H. Ohhata,^{18,*} T. Okamura,^{18,*}
 K. Okumura,⁵⁰ T. Okusawa,³⁵ S.M. Oser,⁵ M. Otani,²⁸ R. A. Owen,³⁹ Y. Oyama,^{18,*}
 T. Ozaki,³⁵ M.Y. Pac,¹² V. Palladino,²³ V. Paolone,³⁸ P. Paul,³⁴ D. Payne,³⁰ G.F. Pearce,⁴⁷
 J.D. Perkin,⁴⁴ V. Pettinacci,¹⁵ F. Pierre,^{8,†} E. Poplawska,³⁹ B. Popov,^{37,¶} M. Posiadala,⁵⁴
 J.-M. Poutissou,⁵² R. Poutissou,⁵² P. Przewlocki,² W. Qian,⁴⁷ J.L. Raaf,⁴ E. Radicioni,²²
 P.N. Ratoff,²⁹ T.M. Raufer,⁴⁷ M. Ravonel,¹⁶ M. Raymond,²¹ F. Retiere,⁵² A. Robert,³⁷
 P.A. Rodrigues,⁴¹ E. Rondio,² J.M. Roney,⁵³ B. Rossi,³ S. Roth,⁴² A. Rubbia,¹⁵
 D. Ruterbories,¹¹ S. Sabouri,⁵ R. Sacco,³⁹ K. Sakashita,^{18,*} F. Sánchez,¹⁹ A. Sarrat,⁸
 K. Sasaki,^{18,*} K. Scholberg,¹³ J. Schwehr,¹¹ M. Scott,²¹ D.I. Scully,⁵⁶ Y. Seiya,³⁵
 T. Sekiguchi,^{18,*} H. Sekiya,⁴⁹ M. Shibata,^{18,*} Y. Shimizu,⁵⁰ M. Shiozawa,⁴⁹ S. Short,²¹
 M. Siyad,⁴⁷ R.J. Smith,³⁶ M. Smy,⁷ J.T. Sobczyk,⁵⁸ H. Sobel,⁷ M. Sorel,²⁰ A. Stahl,⁴²
 P. Stamoulis,²⁰ J. Steinmann,⁴² B. Still,³⁹ J. Stone,⁴ C. Strabel,¹⁵ L.R. Sulak,⁴ R. Sulej,²
 P. Sutcliffe,³⁰ A. Suzuki,²⁷ K. Suzuki,²⁸ S. Suzuki,^{18,*} S.Y. Suzuki,^{18,*} Y. Suzuki,^{18,*}

Y. Suzuki,⁴⁹ T. Szegowski,⁴⁵ M. Szeptycka,² R. Tacik,^{40,52} M. Tada,^{18,*} S. Takahashi,²⁸
A. Takeda,⁴⁹ Y. Takenaga,⁴⁹ Y. Takeuchi,²⁷ K. Tanaka,^{18,*} H.A. Tanaka,^{5,§} M. Tanaka,^{18,*}
M.M. Tanaka,^{18,*} N. Tanimoto,⁵⁰ K. Tashiro,³⁵ I. Taylor,³⁴ A. Terashima,^{18,*} D. Terhorst,⁴²
R. Terri,³⁹ L.F. Thompson,⁴⁴ A. Thorley,³⁰ W. Toki,¹¹ T. Tomaru,^{18,*} Y. Totsuka,^{18,†}
C. Touramanis,³⁰ T. Tsukamoto,^{18,*} M. Tzanov,^{31,10} Y. Uchida,²¹ K. Ueno,⁴⁹ A. Vacheret,²¹
M. Vagins,⁷ G. Vasseur,⁸ T. Wachala,¹⁷ J.J. Walding,²¹ A.V. Waldron,³⁶ C.W. Walter,¹³
P.J. Wanderer,⁶ J. Wang,⁴⁸ M.A. Ward,⁴⁴ G.P. Ward,⁴⁴ D. Wark,^{47,21} M.O. Wascko,²¹
A. Weber,^{36,47} R. Wendell,¹³ N. West,³⁶ L.H. Whitehead,⁵⁶ G. Wikström,¹⁶ R.J. Wilkes,⁵⁷
M.J. Wilking,⁵² J.R. Wilson,³⁹ R.J. Wilson,¹¹ T. Wongjirad,¹³ S. Yamada,⁴⁹ Y. Yamada,^{18,*}
A. Yamamoto,^{18,*} K. Yamamoto,³⁵ Y. Yamanoi,^{18,*} H. Yamaoka,^{18,*} C. Yanagisawa,^{34,**}
T. Yano,²⁷ S. Yen,⁵² N. Yershov,²⁶ M. Yokoyama,⁴⁸ A. Zalewska,¹⁷ J. Zalipska,⁵
L. Zambelli,³⁷ K. Zaremba,⁵⁵ M. Ziembicki,⁵⁵ E.D. Zimmerman,¹⁰ M. Zito,⁸ and J. Żmuda⁵⁸

(The T2K Collaboration)

¹*University of Alberta, Centre for Particle Physics,
Department of Physics, Edmonton, Alberta, Canada*

²*The Andrzej Soltan Institute for Nuclear Studies, Warsaw, Poland*

³*University of Bern, Albert Einstein Center for Fundamental Physics,
Laboratory for High Energy Physics (LHEP), Bern, Switzerland*

⁴*Boston University, Department of Physics, Boston, Massachusetts, U.S.A.*

⁵*University of British Columbia, Department of Physics
and Astronomy, Vancouver, British Columbia, Canada*

⁶*Brookhaven National Laboratory, Physics Department, Upton, New York, U.S.A.*

⁷*University of California, Irvine, Department of
Physics and Astronomy, Irvine, California, U.S.A.*

⁸*IRFU, CEA Saclay, Gif-sur-Yvette, France*

⁹*Chonnam National University, Institute for
Universe & Elementary Particles, Gwangju, Korea*

¹⁰*University of Colorado at Boulder, Department of Physics, Boulder, Colorado, U.S.A.*

¹¹*Colorado State University, Department of Physics, Fort Collins, Colorado, U.S.A.*

¹²*Dongshin University, Department of Physics, Naju, Korea*

- ¹³*Duke University, Department of Physics, Durham, North Carolina, U.S.A.*
- ¹⁴*Ecole Polytechnique, IN2P3-CNRS, Laboratoire Leprince-Ringuet, Palaiseau, France*
- ¹⁵*ETH Zurich, Institute for Particle Physics, Zurich, Switzerland*
- ¹⁶*University of Geneva, Section de Physique, DPNC, Geneva, Switzerland*
- ¹⁷*H. Niewodniczanski Institute of Nuclear Physics PAN, Cracow, Poland*
- ¹⁸*High Energy Accelerator Research Organization (KEK), Tsukuba, Ibaraki, Japan*
- ¹⁹*Institut de Fisica d'Altes Energies (IFAE), Bellaterra (Barcelona), Spain*
- ²⁰*IFIC (CSIC & University of Valencia), Valencia, Spain*
- ²¹*Imperial College London, Department of Physics, London, United Kingdom*
- ²²*INFN Sezione di Bari and Università e Politecnico di Bari, Dipartimento Interuniversitario di Fisica, Bari, Italy*
- ²³*INFN Sezione di Napoli and Università di Napoli, Dipartimento di Fisica, Napoli, Italy*
- ²⁴*INFN Sezione di Padova and Università di Padova, Dipartimento di Fisica, Padova, Italy*
- ²⁵*INFN Sezione di Roma and Università di Roma "La Sapienza", Roma, Italy*
- ²⁶*Institute for Nuclear Research of the Russian Academy of Sciences, Moscow, Russia*
- ²⁷*Kobe University, Kobe, Japan*
- ²⁸*Kyoto University, Department of Physics, Kyoto, Japan*
- ²⁹*Lancaster University, Physics Department, Lancaster, United Kingdom*
- ³⁰*University of Liverpool, Department of Physics, Liverpool, United Kingdom*
- ³¹*Louisiana State University, Department of Physics and Astronomy, Baton Rouge, Louisiana, U.S.A.*
- ³²*Université de Lyon, Université Claude Bernard Lyon 1, IPN Lyon (IN2P3), Villeurbanne, France*
- ³³*Miyagi University of Education, Department of Physics, Sendai, Japan*
- ³⁴*State University of New York at Stony Brook, Department of Physics and Astronomy, Stony Brook, New York, U.S.A.*
- ³⁵*Osaka City University, Department of Physics, Osaka, Japan*
- ³⁶*Oxford University, Department of Physics, Oxford, United Kingdom*
- ³⁷*UPMC, Université Paris Diderot, CNRS/IN2P3, Laboratoire de Physique Nucléaire et de Hautes Energies (LPNHE), Paris, France*
- ³⁸*University of Pittsburgh, Department of Physics and Astronomy, Pittsburgh, Pennsylvania, U.S.A.*

- ³⁹*Queen Mary University of London, School of Physics, London, United Kingdom*
- ⁴⁰*University of Regina, Physics Department, Regina, Saskatchewan, Canada*
- ⁴¹*University of Rochester, Department of Physics
and Astronomy, Rochester, New York, U.S.A.*
- ⁴²*RWTH Aachen University, III. Physikalisches Institut, Aachen, Germany*
- ⁴³*Seoul National University, Department of Physics and Astronomy, Seoul, Korea*
- ⁴⁴*University of Sheffield, Department of Physics and Astronomy, Sheffield, United Kingdom*
- ⁴⁵*University of Silesia, Institute of Physics, Katowice, Poland*
- ⁴⁶*STFC, Daresbury Laboratory, Warrington, United Kingdom*
- ⁴⁷*STFC, Rutherford Appleton Laboratory, Harwell Oxford, United Kingdom*
- ⁴⁸*University of Tokyo, Department of Physics, Tokyo, Japan*
- ⁴⁹*University of Tokyo, Institute for Cosmic Ray
Research, Kamioka Observatory, Kamioka, Japan*
- ⁵⁰*University of Tokyo, Institute for Cosmic Ray Research,
Research Center for Cosmic Neutrinos, Kashiwa, Japan*
- ⁵¹*University of Toronto, Department of Physics, Toronto, Ontario, Canada*
- ⁵²*TRIUMF, Vancouver, British Columbia, Canada*
- ⁵³*University of Victoria, Department of Physics and
Astronomy, Victoria, British Columbia, Canada*
- ⁵⁴*University of Warsaw, Faculty of Physics, Warsaw, Poland*
- ⁵⁵*Warsaw University of Technology, Institute of Radioelectronics, Warsaw, Poland*
- ⁵⁶*University of Warwick, Department of Physics, Coventry, United Kingdom*
- ⁵⁷*University of Washington, Department of Physics, Seattle, Washington, U.S.A.*
- ⁵⁸*Wroclaw University, Faculty of Physics and Astronomy, Wroclaw, Poland*
- ⁵⁹*York University, Department of Physics and Astronomy, Toronto, Ontario, Canada*

(Dated: August 17, 2011)

Abstract

The T2K experiment observes indications of $\nu_\mu \rightarrow \nu_e$ appearance in data accumulated with 1.43×10^{20} protons on target. Six events pass all selection criteria at the far detector. In a three-flavor neutrino oscillation scenario with $|\Delta m_{23}^2| = 2.4 \times 10^{-3} \text{ eV}^2$, $\sin^2 2\theta_{23} = 1$ and $\sin^2 2\theta_{13} = 0$, the expected number of such events is $1.5 \pm 0.3(\text{syst.})$. Under this hypothesis, the probability to observe six or more candidate events is 7×10^{-3} , equivalent to 2.5σ significance. At 90% C.L., the data are consistent with $0.03(0.04) < \sin^2 2\theta_{13} < 0.28(0.34)$ for $\delta_{\text{CP}} = 0$ and normal (inverted) hierarchy.

PACS numbers: 14.60.Pq, 13.15.+g, 25.30.Pt, 95.55.Vj

We report results of a search for ν_e appearance in the T2K experiment [1]. In a three-neutrino mixing scenario, flavor oscillations are described by the PMNS matrix [2, 3], usually parametrized by the three angles θ_{12} , θ_{23} , θ_{13} , and the CP -violating phase δ_{CP} . Previous experiments have observed neutrino oscillations driven by θ_{12} and θ_{23} in the solar (Δm_{12}^2) and atmospheric ($\Delta m_{13}^2 \simeq \Delta m_{23}^2$) sectors [4–9]. In the atmospheric sector, data are consistent with $|\Delta m_{23}^2| \simeq 2.4 \times 10^{-3} \text{ eV}^2$, a normal $\Delta m_{23}^2 > 0$ or inverted $\Delta m_{23}^2 < 0$ mass hierarchy, and $\sin^2 2\theta_{23}$ close to, or equal to unity. Searches for oscillations driven by θ_{13} have been inconclusive and upper limits have been derived [10–13], with the most stringent being $\sin^2 2\theta_{13} < 0.15$ (90%C.L.), set by CHOOZ [14] and MINOS [15].

T2K uses a conventional neutrino beam produced at J-PARC and directed 2.5° off-axis to Super-Kamiokande (SK) at a distance $L = 295 \text{ km}$. This configuration produces a narrow-band ν_μ beam [16], tuned at the first oscillation maximum $E_\nu = |\Delta m_{23}^2| L / (2\pi) \simeq 0.6 \text{ GeV}$, reducing backgrounds from higher energy neutrino interactions.

Details of the T2K experimental setup are described elsewhere [17]. Here we briefly review the components relevant for the ν_e search. The J-PARC Main Ring (MR) accelerator [18] provides 30 GeV protons with a cycle of 0.3 Hz. Eight bunches are single-turn extracted in $5 \mu\text{s}$ and transported through an extraction line arc defined by superconducting combined-function magnets to the production target. The primary beamline is equipped with 21 electrostatic beam position monitors (ESM), 19 segmented secondary emission monitors (SSEM), one optical transition radiation monitor (OTR) and five current transformers. The secondary beamline, filled with He at atmospheric pressure, is composed of the target, focusing horns and decay tunnel. The graphite target is 2.6 cm in diameter and 90 cm ($1.9\lambda_{int}$) long. Charged particles exiting the target are sign selected and focused into the 96 m long decay tunnel by three magnetic horns pulsed at 250 kA. Neutrinos are primarily produced in the decays of charged pions and kaons. A beam dump is located at the end of the tunnel and is followed by muon monitors.

The Near Detector complex [17] located 280 m downstream from the target hosts two detectors. The on-axis Interactive Neutrino GRID (INGRID) accumulates neutrino interactions with high statistics to monitor the beam intensity, direction and profile. It consists of 14 identical 7-ton iron-absorber/scintillator-tracker sandwich modules arranged in 10 m by 10 m crossed horizontal and vertical arrays centered on the beam. The off-axis detector reconstructs exclusive final states to study neutrino interactions and beam properties corre-

sponding to those expected at the far detector. Embedded in the refurbished UA1 magnet (0.2 T), it consists of three large volume time projection chambers (TPCs) [19] interleaved with two fine-grained tracking detectors (FGDs, each 1 ton), a π^0 -optimized detector and a surrounding electromagnetic calorimeter. The magnet yoke is instrumented as a side muon range detector.

The SK water Cherenkov far detector [20] has a fiducial volume (FV) of 22.5 kton within its cylindrical inner detector (ID). Enclosing the ID all around is the 2 m-wide outer detector (OD). The front-end readout electronics allow for a zero-deadtime software trigger. Spill timing information, synchronized by the Global Positioning System (GPS) with < 150 ns precision, is transferred online to SK and triggers the recording of photomultiplier hits within $\pm 500 \mu\text{s}$ of the expected arrival time of the neutrinos.

The results presented in this Letter are based on the first two physics runs: Run 1 (Jan–Jun 2010) and Run 2 (Nov 2010–Mar 2011). During this time period, the MR proton beam power was continually increased and reached 145 kW with 9×10^{13} protons per pulse. The targeting efficiency was monitored by the ESM, SSEM and OTR and found to be stable at over 99%. The muon monitors provided additional spill-by-spill steering information. A total of 2,474,419 spills were retained for analysis after beam and far detector quality cuts, yielding 1.43×10^{20} protons on target (p.o.t.).

We present the study of events in the far detector with only a single electron-like (e -like) ring. The analysis produces a sample enhanced in ν_e charged-current quasi-elastic interactions (CCQE) arising from $\nu_\mu \rightarrow \nu_e$ oscillations. The main backgrounds are intrinsic ν_e contamination in the beam and neutral current (NC) interactions with a misidentified π^0 . The selection criteria for this analysis were fixed from Monte Carlo (MC) studies before the data were collected, optimized for the initial running conditions. The observed number of events is compared to expectations based on neutrino flux and cross-section predictions for signal and all sources of backgrounds, which are corrected using an inclusive ν_μ charged-current (CC) measurement in the off-axis near detector.

We compute the neutrino beam fluxes (Fig. 1) starting from models and tuning them to experimental data. Pion production in (p, θ) bins is based on the NA61 measurements [21], typically with 5–10% uncertainties. Pions produced outside the experimentally measured phase space, as well as kaons, are modeled using FLUKA [22, 23]. These pions are assigned systematic uncertainties on their production of 50%, while kaon production uncertainties,

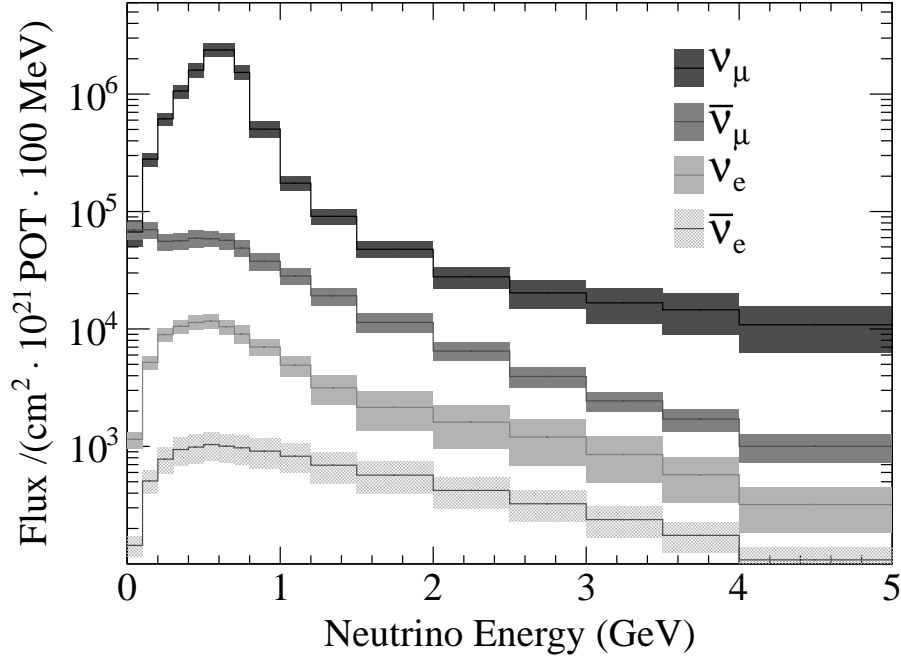


FIG. 1. Predicted neutrino fluxes at the far detector, in absence of oscillations. The shaded boxes indicate the total systematic uncertainties for each energy bin.

estimated from a comparison with data from Eichten *et al.* [24], range from 15% to 100% depending on the bin. GEANT3 [25], with GCALOR [26] for hadronic interactions, handles particle propagation through the magnetic horns, target hall, decay volume and beam dump. Additional errors to the neutrino fluxes are included for the proton beam uncertainties, secondary beamline component alignment uncertainties, and the beam direction uncertainty.

The neutrino beam profile and its absolute rate (1.5 events/ 10^{14} p.o.t.) as measured by INGRID were stable and consistent with expectations. The beam profile center (Fig. 2) indicates that beam steering was better than ± 1 mrad. The correlated systematic error is $\pm 0.33(0.37)$ mrad for the horizontal(vertical) direction. The error on the SK position relative to the beamline elements was obtained from a dedicated GPS survey and is negligible. As shown in Fig. 1, the estimated uncertainties of the intrinsic ν_μ and ν_e fluxes below 1 GeV are around 14%. Above 1 GeV, the intrinsic ν_e flux error is dominated by the uncertainty on the kaon production rate with resulting errors of 20–50%.

The NEUT MC event generator [28], which has been tuned with recent neutrino interaction data in an energy region compatible with T2K [29–31], is used to simulate neutrino interactions in the near and far detectors. The GENIE [32] generator provides a separate

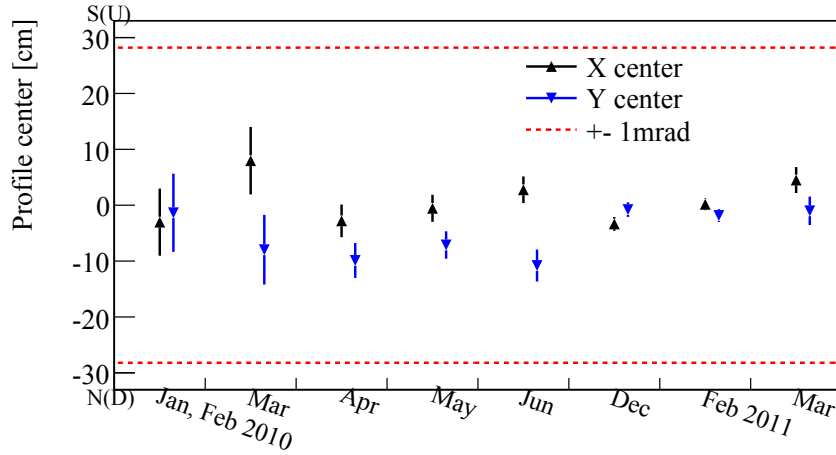


FIG. 2. Beam centering stability in horizontal (x, South–North) and vertical (y, Down–Up) directions as a function of time, as measured by INGRID. Errors shown are only statistical. The dashed lines correspond to a change of beam direction by ± 1 mrad.

TABLE I. Summary of systematic uncertainties for the relative rate of different charged-current (CC) and neutral-current (NC) reactions to the rate for CCQE.

Process	Systematic error
CCQE	energy-dependent (7% at 500 MeV)
CC 1π	30% ($E_\nu < 2$ GeV) – 20% ($E_\nu > 2$ GeV)
CC coherent π^\pm	100% (upper limit from [27])
CC other	30% ($E_\nu < 2$ GeV) – 25% ($E_\nu > 2$ GeV)
NC $1\pi^0$	30% ($E_\nu < 1$ GeV) – 20% ($E_\nu > 1$ GeV)
NC coherent π	30%
NC other π	30%
FSI	energy-dependent (10% at 500 MeV)

cross-check of the assumed cross-sections and uncertainties, and yields consistent results. A list of reactions and their uncertainties relative to the CCQE total cross-section is shown in Table I. An energy-dependent error on CCQE is assigned to account for the uncertainty in the low energy cross-section, especially for the different target materials between the near and far detectors. Uncertainties in intranuclear final state interactions (FSI), implemented with a microscopic cascade model [33], introduce an additional error in the rates (see e.g.

[34]).

An inclusive ν_μ CC measurement in the off-axis near detector is used to constrain the expected event rate at the far detector. From a data sample collected in Run 1 and corresponding to 2.88×10^{19} p.o.t. after detector quality cuts, neutrino interactions are selected in the FGDs with tracks entering the downstream TPC. The most energetic negative track in the TPC is chosen and we require its ionization loss to be compatible with a muon. To reduce background from interactions outside the FGDs, there must be no track in the upstream TPC. The analysis selects 1529 data events (38% ν_μ CC efficiency for 90% purity, estimated from MC). The momentum distribution of the selected muons (Fig. 3) shows good agreement between data and MC. The measured data/MC ratio is

$$R_{ND}^{\mu,Data}/R_{ND}^{\mu,MC} = 1.036 \pm 0.028(\text{stat.})_{-0.037}^{+0.044}(\text{det.syst.}) \pm 0.038(\text{phys.syst.}), \quad (1)$$

where $R_{ND}^{\mu,Data}$ and $R_{ND}^{\mu,MC}$ are the p.o.t. normalized rates of ν_μ CC interactions in data and MC. The detector systematic errors mainly come from tracking and particle identification efficiencies, and physics uncertainties are related to the interaction modeling. Uncertainties that effectively cancel between near and far detectors were omitted.

At the far detector, we extract a fully-contained fiducial volume (FCFV) sample by requiring no event activity in either the OD or in the 100 μs before the event trigger time, at least 30 MeV electron-equivalent energy deposited in the ID (defined as visible energy E_{vis}), and the reconstructed vertex in the fiducial region. The data have 88 such FCFV events that are within the timing range from -2 to $10 \mu\text{s}$ around the beam trigger time. The accidental contamination from non-beam related events is determined from the sidebands to be 0.003 events. A Kolmogorov-Smirnov (KS) test of the observed number of FCFV events as a function of accumulated p.o.t. is compatible with the normalized event rate being constant ($p\text{-value}=0.32$). The analysis relies on the well-established reconstruction techniques developed for other data samples [4]. Forty-one events are reconstructed with a single ring, and eight of those are e -like. Six of these events have $E_{vis} > 100$ MeV and no delayed-electron signal. To suppress misidentified π^0 mesons, the reconstruction of two rings is forced by comparison of the observed and expected light patterns calculated under the assumption of two showers [35], and a cut on the two-ring invariant mass $M_{inv} < 105 \text{ MeV}/c^2$ is imposed. No events are rejected (Fig. 4). Finally, the neutrino energy E_ν^{rec} is computed using the reconstructed momentum and direction of the ring, by assuming

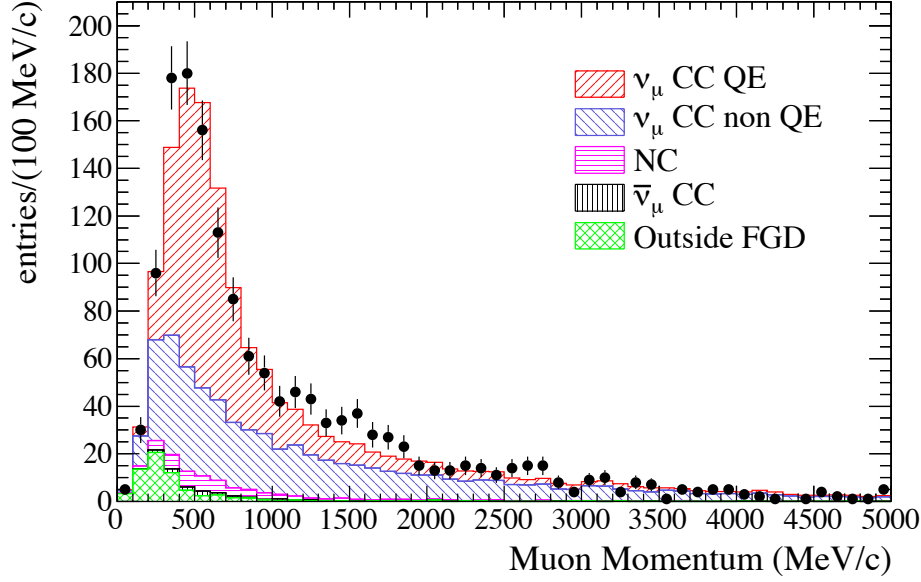


FIG. 3. Measured muon momentum of ν_μ CC candidates reconstructed in the FGD target. The data are shown using points with error bars (statistical only) and the MC predictions are in histograms shaded according to their type.

quasi-elastic kinematics and neglecting Fermi motion. No events are rejected by requiring $E_\nu^{rec} < 1250$ MeV, aimed at suppressing events from the intrinsic ν_e component arising primarily from kaon decays (Fig. 5). The data and MC reductions after each selection criterion are shown in Table II. The ν_e appearance signal efficiency is estimated from MC to be 66% while rejection for $\nu_\mu + \bar{\nu}_\mu$ CC, intrinsic ν_e CC, and NC are $> 99\%$, 77%, and 99%, respectively. Of the surviving background NC interactions constitute 46%, of which 74% are due to π^0 mesons and 6% originate from single gamma production.

Examination of the six data events shows properties consistent with ν_e CC interactions. The distribution of the cosine of the opening angle between the ring and the incoming beam direction is consistent with CCQE events. The event vertices in cylindrical coordinates (R, ϕ, z) show that these events are clustered at large R , near the edge of the FV in the upstream beam direction. A KS test on the R^2 distribution of our final events yields a p -value of 0.03. If this was related to contamination from penetrating particles produced in upstream neutrino interactions, then the ID region outside the FV should show evidence for such events, however this is not observed. In addition, an analysis of the neutrino interactions occurring in the OD volume is consistent with expectations.

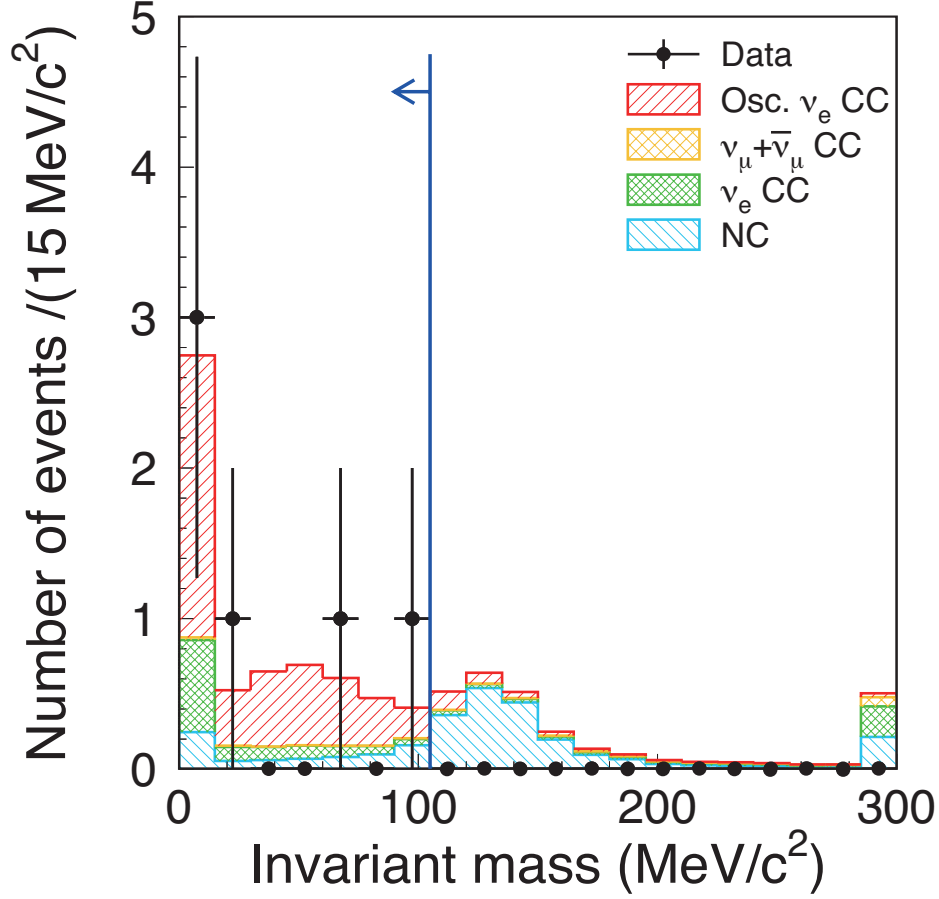


FIG. 4. Distribution of invariant mass M_{inv} when each event is forced to be reconstructed into two rings. The data are shown using points with error bars (statistical only) and the MC predictions are in shaded histograms, corresponding to oscillated ν_e CC signal and various background sources for $\sin^2 2\theta_{13} = 0.1$. The last bin shows overflow entries. The vertical line shows the applied cut at $105 \text{ MeV}/c^2$.

To compute the expected number of events at the far detector N_{SK}^{exp} , we use the near detector ν_μ CC interaction rate measurement as normalization, and the ratio of expected events in the near and far detectors, where common systematic errors cancel. Using Eq. 1, this can be expressed as:

$$N_{SK}^{exp} = \left(R_{ND}^{\mu, Data} / R_{ND}^{\mu, MC} \right) \cdot N_{SK}^{MC}, \quad (2)$$

where N_{SK}^{MC} is the MC number of events expected in the far detector. Due to the correlation of systematic errors in the near and far detector samples, Eq. 2 reduces the uncertainty on the expected number of events. Event rates are computed incorporating three-flavor oscillation

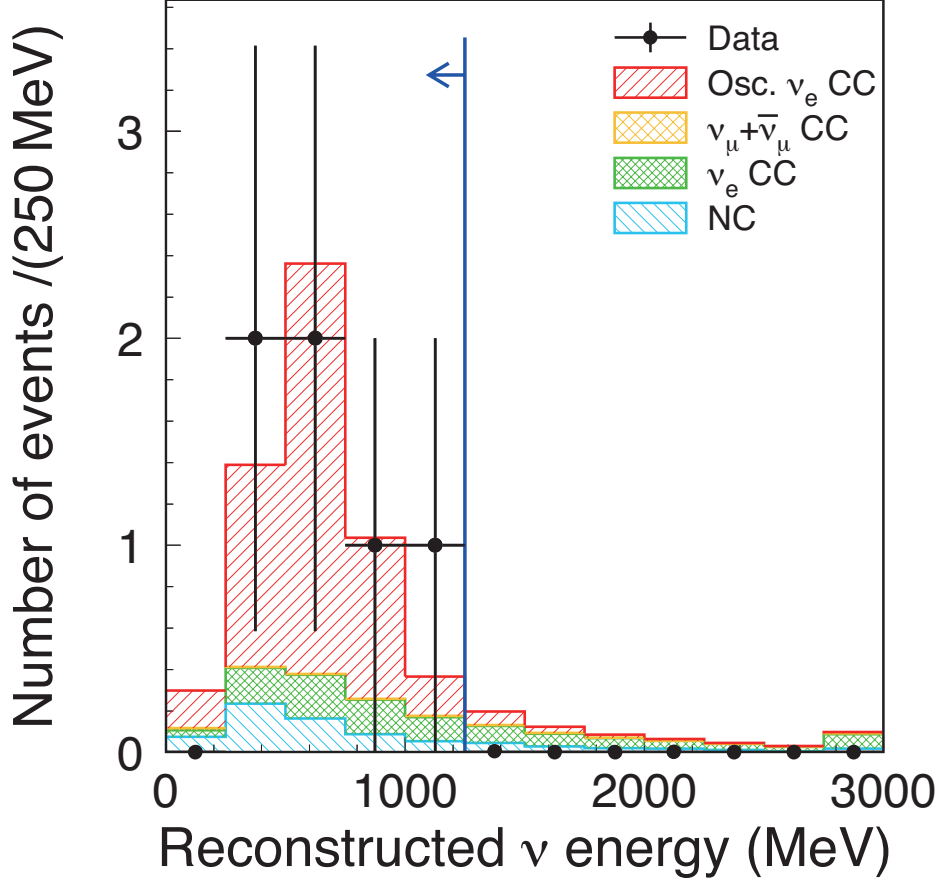


FIG. 5. Same as Fig. 4 for the reconstructed neutrino energy spectrum of the events which pass all ν_e appearance signal selection criteria with the exception of the energy cut. The vertical line shows the applied cut at 1250 MeV.

probabilities and matter effects [36] with $\Delta m_{12}^2 = 7.6 \times 10^{-5} \text{ eV}^2$, $\Delta m_{23}^2 = +2.4 \times 10^{-3} \text{ eV}^2$, $\sin^2 2\theta_{12} = 0.8704$, $\sin^2 2\theta_{23} = 1.0$, an average Earth density $\rho = 3.2 \text{ g/cm}^3$ and $\delta_{\text{CP}} = 0$ unless otherwise noted. The expectations are 0.03(0.03) $\nu_\mu + \bar{\nu}_\mu$ CC, 0.8(0.7) intrinsic ν_e CC, and 0.1(4.1) $\nu_\mu \rightarrow \nu_e$ oscillation events for $\sin^2 2\theta_{13} = 0(0.1)$, and 0.6 NC events. As shown in Table III, the total systematic uncertainty on N_{SK}^{exp} depends on θ_{13} . Neutrino flux uncertainties contribute 14.9%(15.4%) to the far(near) event rates, but their ratio has an 8.5% error due to cancellations. The near detector ν_μ CC selection efficiency uncertainty yields $^{+5.6\%}_{-5.2\%}$ and the statistical uncertainty gives 2.7%. The errors from cross-section modeling are dominated by FSI uncertainties and by the knowledge of the $\sigma(\nu_e)/\sigma(\nu_\mu)$ ratio, estimated to $\pm 6\%$. The systematic uncertainties due to event selection in SK were studied with cosmic-ray muons, electrons from muon decays, and atmospheric neutrino events. Their contribution

TABLE II. Event reduction for the ν_e appearance search at the far detector. After each selection criterion is applied, the numbers of observed (Data) and MC expected events of ν_μ CC, intrinsic ν_e CC, NC, and the ν_e CC signal, are given. All MC CC samples include three-flavor oscillations for $\sin^2 2\theta_{13}=0.1$ and $\delta_{\text{CP}} = 0$.

	Data	ν_μ CC	ν_e CC	NC	$\nu_\mu \rightarrow \nu_e$ CC
(0) interaction in FV	n/a	67.2	3.1	71.0	6.2
(1) fully-contained FV	88	52.4	2.9	18.3	6.0
(2) single ring	41	30.8	1.8	5.7	5.2
(3) e -like	8	1.0	1.8	3.7	5.2
(4) $E_{vis} > 100$ MeV	7	0.7	1.8	3.2	5.1
(5) no delayed electron	6	0.1	1.5	2.8	4.6
(6) non- π^0 -like	6	0.04	1.1	0.8	4.2
(7) $E_\nu^{rec} < 1250$ MeV	6	0.03	0.7	0.6	4.1

to $\delta N_{SK}^{exp}/N_{SK}^{exp}$ for e.g. $\sin^2 2\theta_{13} = 0.1$ is as follows: 1.4% from the fiducial volume definition, 0.6% from the energy scale and 0.2% from the delayed electron signal tagging efficiency. The π^0 rejection efficiency, studied with a NC π^0 topological control sample combining one data electron and one simulated gamma event, contributes 0.9%. The uncertainty on the acceptance of one-ring e -like events was studied with an atmospheric neutrino sample, adding a contribution of 5% from ring counting and 4.9% from particle identification uncertainties. The performance of muon rejection by the ring particle identification algorithm was investigated using cosmic-ray muons and atmospheric neutrino events, giving 0.3%. The effect from uncertainties in the M_{inv} cut is 6.0%. Combining the above uncertainties, the total far detector systematic error contribution to $\delta N_{SK}^{exp}/N_{SK}^{exp}$ is 14.7%(9.4%) for $\sin^2 2\theta_{13} = 0(0.1)$.

Our oscillation result is based entirely on comparing the number of ν_e candidate events with predictions, varying $\sin^2 2\theta_{13}$ for each δ_{CP} value. Including systematic uncertainties, the expectation is $1.5 \pm 0.3 (5.5 \pm 1.0)$ events for $\sin^2 2\theta_{13} = 0(0.1)$. At each oscillation parameter point, a probability distribution for the expected number of events is constructed, incorporating systematic errors [37], which is used to make the confidence interval (Fig. 6), following the unified ordering prescription of Feldman and Cousins [38].

In conclusion, the observation of six single ring e -like events exceeds the expectation of

TABLE III. Contributions from various sources and the total relative uncertainty for $\sin^2 2\theta_{13}=0$ and 0.1, and $\delta_{\text{CP}} = 0$.

Source	$\sin^2 2\theta_{13} = 0$	$\sin^2 2\theta_{13} = 0.1$
(1) neutrino flux	$\pm 8.5\%$	$\pm 8.5\%$
(2) near detector	$^{+5.6\%}_{-5.2\%}$	$^{+5.6\%}_{-5.2\%}$
(3) near det. statistics	$\pm 2.7\%$	$\pm 2.7\%$
(4) cross section	$\pm 14.0\%$	$\pm 10.5\%$
(5) far detector	$\pm 14.7\%$	$\pm 9.4\%$
Total $\delta N_{SK}^{\text{exp}}/N_{SK}^{\text{exp}}$	$^{+22.8\%}_{-22.7\%}$	$^{+17.6\%}_{-17.5\%}$

a three-flavor neutrino oscillation scenario with $\sin^2 2\theta_{13} = 0$. Under this hypothesis, the probability to observe six or more candidate events is 7×10^{-3} . Thus, we conclude that our data indicate ν_e appearance from a ν_μ neutrino beam. This result converted into a confidence interval yields $0.03(0.04) < \sin^2 2\theta_{13} < 0.28(0.34)$ at 90% C.L. for $\sin^2 2\theta_{23} = 1.0$, $|\Delta m_{23}^2| = 2.4 \times 10^{-3} \text{ eV}^2$, $\delta_{\text{CP}} = 0$ and for normal (inverted) neutrino mass hierarchy. Under the same assumptions, the best fit points are 0.11(0.14), respectively. For non-maximal $\sin^2 2\theta_{23}$, the confidence intervals remain unchanged to first order by replacing $\sin^2 2\theta_{13}$ by $2 \sin^2 \theta_{23} \sin^2 2\theta_{13}$. More data are required to firmly establish ν_e appearance and to better determine the angle θ_{13} .

We thank the J-PARC accelerator team for the superb accelerator performance and CERN NA61 colleagues for providing essential particle production data and for their excellent collaboration. We acknowledge the support of MEXT, Japan; NSERC, NRC and CFI, Canada; CEA and CNRS/IN2P3, France; DFG, Germany; INFN, Italy; Ministry of Science and Higher Education, Poland; RAS, RFBR and the Ministry of Education and Science of the Russian Federation; MEST and NRF, South Korea; MICINN and CPAN, Spain; SNSF and SER, Switzerland; STFC, U.K.; and DOE, U.S.A. We also thank CERN for their donation of the UA1/NOMAD magnet and DESY for the HERA-B magnet mover system. In addition, participation of individual researchers and institutions in T2K has been further supported by funds from: ERC (FP7), EU; JSPS, Japan; Royal Society, UK; DOE-OJI and DOE-Early Career program, and the A. P. Sloan Foundation, U.S.A.

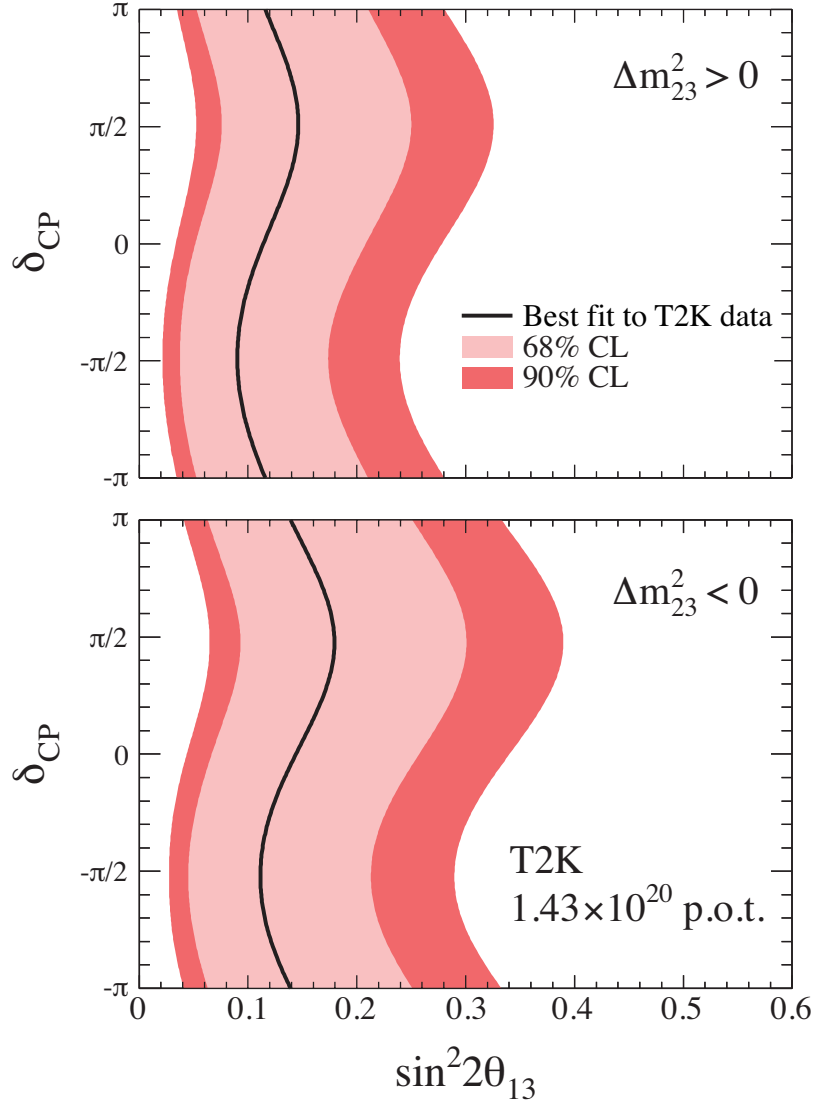


FIG. 6. The 68% and 90% C.L. regions for $\sin^2 2\theta_{13}$ for each value of δ_{CP} , consistent with the observed number of events in the three-flavor oscillation case for normal (top) and inverted (bottom) mass hierarchy. The other oscillation parameters are fixed (see text). The best fit values are shown with solid lines.

* also at J-PARC Center

[†] deceased

[‡] now at CERN

[§] also at Institute of Particle Physics, Canada

[¶] also at JINR, Dubna, Russia

^{**} also at BMCC/CUNY, New York, New York, U.S.A.

- [1] Y. Itow *et al.* (T2K Collaboration), (2001), arXiv:hep-ex/0106019.
- [2] Z. Maki, M. Nakagawa, and S. Sakata, Prog. Theor. Phys. **28**, 870 (1962).
- [3] B. Pontecorvo, Sov. Phys. JETP **26**, 984 (1968).
- [4] Y. Ashie *et al.* (Super-Kamiokande Collaboration), Phys. Rev. **D71**, 112005 (2005), hep-ex/0501064.
- [5] J. Hosaka *et al.* (Super-Kamiokande Collaboration), Phys.Rev. **D73**, 112001 (2006), hep-ex/0508053.
- [6] B. Aharmim *et al.* (SNO Collaboration), Phys. Rev. **C72**, 055502 (2005), nucl-ex/0502021.
- [7] M. H. Ahn *et al.* (K2K Collaboration), Phys. Rev. **D74**, 072003 (2006), arXiv:hep-ex/0606032.
- [8] S. Abe *et al.* (KamLAND Collaboration), Phys.Rev.Lett. **100**, 221803 (2008), arXiv:0801.4589 [hep-ex].
- [9] P. Adamson *et al.* (MINOS Collaboration), Phys. Rev. Lett. **106**, 181801 (2011), arXiv:1103.0340 [hep-ex].
- [10] S. Yamamoto *et al.* (K2K Collaboration), Phys.Rev.Lett. **96**, 181801 (2006), arXiv:hep-ex/0603004 [hep-ex].
- [11] R. Wendell *et al.* (Super-Kamiokande Collaboration), Phys.Rev. **D81**, 092004 (2010), arXiv:1002.3471 [hep-ex].
- [12] B. Aharmim *et al.* (SNO Collaboration), Phys.Rev. **C81**, 055504 (2010), arXiv:0910.2984 [nucl-ex].
- [13] A. Gando *et al.* (KamLAND Collaboration), Phys.Rev. **D83**, 052002 (2011), arXiv:1009.4771 [hep-ex].
- [14] M. Apollonio *et al.* (Chooz Collaboration), Eur. Phys. J. **C27**, 331 (2003), hep-ex/0301017.
- [15] P. Adamson *et al.* (MINOS Collaboration), Phys.Rev. **D82**, 051102 (2010), arXiv:1006.0996 [hep-ex].
- [16] D. Beavis, A. Carroll, I. Chiang, et al. (E889 Collaboration), Physics Design Report **BNL 52459** (1995).

- [17] K. Abe *et al.* (T2K Collaboration), (2011), 10.1016/j.nima.2011.06.067, accepted for publication in Nucl. Instrum. Methods, article in press, arXiv:1106.1238 [physics.ins-det].
- [18] Y. Yamazaki *et al.*, KEK Report 2002-13 and JAERI-Tech 2003-44 and J-PARC-03-01 (2003).
- [19] N. Abgrall *et al.*, Nucl. Instrum. Meth. **A637**, 25 (2011), arXiv:1012.0865 [physics.ins-det].
- [20] Y. Fukuda *et al.* (Super-Kamiokande Collaboration), Nucl. Instrum. Meth. **A501**, 418 (2003).
- [21] N. Abgrall *et al.* (NA61/SHINE Collaboration), submitted to Phys.Rev.C (2011), arXiv:1102.0983 [hep-ex].
- [22] A. Ferrari, P. R. Sala, A. Fasso, and J. Ranft, (2005), CERN-2005-010 and SLAC-R-773 and INFN-TC-05-11.
- [23] G. Battistoni *et al.*, AIP Conf. Proc. **896**, 31 (2007).
- [24] T. Eichten *et al.*, Nucl. Phys. B **44**, 333 (1972).
- [25] R. Brun, F. Carminati, and S. Giani, (1994), CERN-W5013.
- [26] C. Zeitnitz and T. A. Gabriel, In Proc. of International Conference on Calorimetry in High Energy Physics, Tallahassee, FL, USA, February 1993.
- [27] K. Hiraide *et al.* (SciBooNE Collaboration), Phys.Rev. **D78**, 112004 (2008), arXiv:0811.0369 [hep-ex].
- [28] Y. Hayato, Nucl.Phys.(Proc. Suppl.) **B112**, 171 (2002).
- [29] Y. Nakajima *et al.* (SciBooNE Collaboration), Phys.Rev. **D83**, 012005 (2011), arXiv:1011.2131 [hep-ex].
- [30] A. Aguilar-Arevalo *et al.* (MiniBooNE Collaboration), Phys.Rev. **D81**, 092005 (2010), arXiv:1002.2680 [hep-ex].
- [31] Y. Kurimoto *et al.* (SciBooNE Collaboration), Phys.Rev. **D81**, 033004 (2010), arXiv:0910.5768 [hep-ex].
- [32] C. Andreopoulos, A. Bell, D. Bhattacharya, F. Cavanna, J. Dobson, *et al.*, Nucl.Instrum.Meth. **A614**, 87 (2010), arXiv:0905.2517 [hep-ph].
- [33] L. L. Salcedo *et al.*, Nucl.Phys. **A484**, 557 (1988).
- [34] T. S. H. Lee and R. P. Redwine, Annu.Rev.Nucl. **52**, 23 (2002).
- [35] T. Barszczak, (2005), Ph.D. Thesis (University of California, Irvine), UMI-31-71221.
- [36] V. Barger, K. Whisnant, S. Pakvasa, and R. J. N. Phillips, Phys. Rev. D **22**, 2718 (1980).
- [37] J. Conrad, O. Botner, A. Hallgren, and C. Perez de los Heros, Phys.Rev. **D67**, 012002 (2003), arXiv:hep-ex/0202013 [hep-ex].

[38] G. J. Feldman and R. D. Cousins, Phys. Rev. D **57**, 3873 (1998).